Simulation of the ATLAS SCT barrel module response to LHC beam loss scenarios

P. Rose,[*] A.A. Grillo, V. Fadeyev, E. Spencer, M. Wilder and M. Domingo

Santa Cruz Institute for Particle Physics, University of California Santa Cruz, 1156 High Street, Santa Cruz, CA 95064, U.S.A

E-mail: prose@ucsc.edu

ABSTRACT: In the event of beam loss at the LHC, ATLAS Inner Detector components nearest the beam line may be subjected to unusually large amounts of radiation. Understanding their behavior in such an event is important in determining whether they would still function properly. We built a SPICE model of the silicon strip module electrical system to determine the behavior of its elements during a realistic beam loss scenario. We found that the power supply and bias filter characteristics strongly affect the module response in such scenarios. In particular, the following self-limiting phenomena were observed: there is a finite amount of charge initially available on the bias filter capacitors for collection by the strips; the power supply current limit reduces the rate at which the bias filter capacitors' charge can be replenished; the reduced bias voltage leads to a smaller depletion depth in the sensors which results in less collected charge. These effects provide a larger measure of safety during beam loss events than was previously assumed. In particular, the voltage across the coupling capacitor stays below the specifications limit for a wide range of beam loss rates. The current into the ABCD channels exceeds the limit only for very high rates of beam loss.

KEYWORDS: LHC Beam Loss, ATLAS SCT Barrel Module

ATL-INDET-PROC-2013-013
29 October 2013

[*] Corresponding author.

Contents

1. Introduction

The Large Hadron Collider (LHC) is a particle accelerator near Geneva, Switzerland, that collides beams of protons in two concentric rings at four separate interaction points with a design center-of-mass energy of 14 TeV. At design luminosity, the LHC will contain in each ring approximately 2,000 bunches with each bunch containing 100 billion protons and each bunch separated by 25 ns. In the event that the beam is misteered, a fraction of them may scrape the beam pipe or collimators, resulting in a large flux of secondary particles into the detectors at each interaction point. The purpose of the work presented here is to determine the effect of these scenarios on the ATLAS SemiConductor Tracker.

The ATLAS [1] SemiConductor Tracker (SCT) is an essential sub-system of the ATLAS Inner Detector, which tracks charged particles resulting from collisions at the LHC. The SCT contains both barrel [2] and endcap regions, with 2112 modules comprising the barrel region. There are four silicon strip sensors per double-sided barrel module, each containing 768 individual strips. The strips on each side of a given module are daisy-chained together to make an effective combination of 1536 12-cm strips per module. All components inside the detector volume have been thoroughly tested for radiation hardness such that the extra radiation damage from a beam loss can be tolerated. However, both the ABCD readout IC [3] and the coupling capacitors between the implant and readout strips may experience problems from a large instantaneous charge deposition. The ABCD is rated to handle up to 5 nC in 25 ns, but previous tests have shown that it can withstand at least twice that amount [4]. The coupling capacitor is rated to 100 V and DC tests have confirmed it is safe up to this threshold. In fact, higher values have been observed with no apparent damage [4, 5], but since all sensors have only been systematically tested up to 100 V, this is still considered the safe reference limit.

Previous simulations have shown that during the most likely beam loss scenarios, the SCT barrel modules may experience a large particle flux of up to 5.4×10^5 MIPs (minimum ionizing particles) per strip per bunch crossing [6]. That study did not address the effect of multiple, successive bunches scraping the beam pipe or collimators and the resulting effects on the SCT components. To systematically investigate this issue, we have built a detailed SPICE model (using the LTSpice [7] simulator). of the SCT barrel module electrical system and simulated scenarios where the particle flux increases linearly from 0 to 5.4×10^5 MIPs/strip/bunch crossing over time scales ranging from 100 ms to 10 ns before a beam dump is initiated.

2. The SPICE model for a barrel module

2.1 Power supply, cables, and bias filter

A schematic of the barrel module electrical system is shown in the lower portion of Figure 1. The bias voltage source supplies up to 500 V and is current limited to 5.2 mA by an internal feedback loop. Once this limit is reached, the output voltage is reduced accordingly to keep the current at or below this limit. In our model, this voltage source is implemented as an ideal voltage source in series with a current limiting diode. Once the 5.2 mA limit is reached, a voltage drop occurs across the diode, thus mimicking the real voltage source by reducing the effective output voltage.

In the experimental setup, the power supply is separated from the bias filter by 100 m of cable. We used a 10-segment distributed RLC circuit to model the cable. The values for

resistance, inductance, and capacitance are 0.117 Ω/m, 7.05 nH/cm, and 0.35 pF/cm, respectively.

The bias filter is implemented as a network of resistors and capacitors and matches its circuit diagram. Each capacitor has a value of 50 nF. The two resistors separating the voltage source output from the sensor backplane each have a value of 5 kΩ, and the single resistor separating the voltage return line from ground has a value of 1 kΩ. There are two additional capacitors across the high voltage and return line in our model to account for bypass capacitors at each of the patch panels (PP1 and 3). A 15 nF capacitor is added at the cable/bias filter junction for PP1, and a 54 nF capacitor is added at the fourth cable node from the cable/bias filter junction for PP3. The bias filter is then connected directly to the sensor backplane.

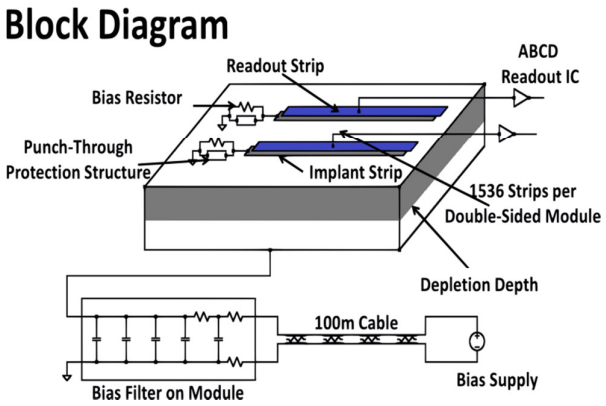

Figure 1: Block diagram of an SCT barrel module that outlines features of our model.

2.2 Silicon strips

The upper portion of Figure 1 outlines the important features of the silicon strip detectors that are incorporated into our model, and Figure 2 shows the SPICE implementation of each strip. Starting from the backplane, we first modeled the sensor bulk using a combination of current sources for charge collection, resistors for leakage current, and capacitors for the backplane to implant strip capacitance. Each charge collection mechanism consists of three current sources. The current sources connecting the backplane to the implant-strip nodes model the timing structure of the beam. These produce the expected collected current per strip for a given particle flux, assuming the bias voltage remains above its full depletion value. The additional current sources, which connect each side of the main current sources to ground, model the dependence of collected charge on the bias voltage. For bias voltages below the full depletion value, we expect the amount of charge collected per strip to decrease according to,

$$I(t) = I_0(t)\sqrt{V_{bias}/V_{fd}} \quad (1)$$

where $I_0(t)$ is the expected current assuming no dependence on bias voltage, V_{bias} is the voltage difference between the backplane and implant strip node, and V_{fd} is the full depletion voltage. The excess current, $I_0(t) - I(t)$, is removed and deposited back into ground by the additional current sources so as to not affect other components in the simulation.

Both the implant strip and the readout strip are modeled with resistors. The implant strip has a resistance of 85 kΩ/cm, and the readout strip has a resistance of 8.9 Ω/cm. On one end of each implant strip there is a 1.35 MΩ bias resistor in parallel with a punch-through protection (PTP) structure. For implant voltages above a certain threshold, the PTP provides a voltage-

dependent resistive path to ground, which is designed to limit high voltages on the implant strips. We used a current-dependent current source to model the PTP. This current source senses the bias resistor current and then adjusts its own value so that the effective resistance of the parallel combination matches our measurements made on SCT production sensors. A layer of dielectric separates the implant and readout strips so that these are capacitively coupled with a capacitance of 23.5 pF/cm, and this layer is rated to withstand 100 V.

We have simulated two types of the sensor performance: 1) non-irradiated sensor with 150 V full depletion voltage, biased at 350 V; 2) irradiated sensor at the end of SCT lifetime with 350 V depletion voltage, biased at 480 V [8].

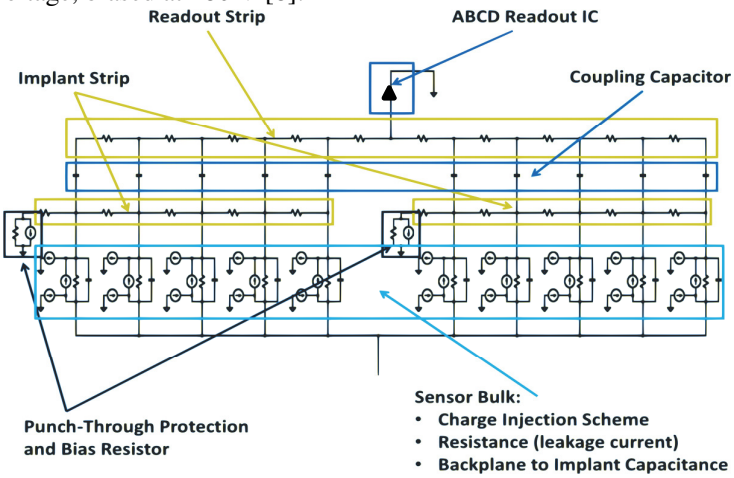

Figure 2: SPICE model of a silicon strip.

The final component of our strip model is the ABCD readout IC. We model each channel of the amplifier as a separate circuit connected to the circuit representing the sensor strip. We have previously measured the ABCD response to voltage signals using a "zapper" circuit that was capable of both short and long pulses [4]. The short pulse could reach a maximum of 80 V with a 40 ns transition time, and the long pulse could reach 450 V with a 1 μs transition time.

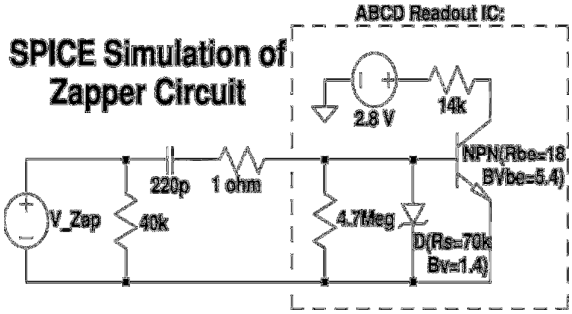

Figure 3: SPICE simulation of the zapper circuit showing our model for the ABCD readout IC.

The ABCD response to both of these signals motivated our model consisting of an NPN transistor with both a large resistor and a Zener diode in parallel with its base-emitter junction. The SPICE parameters for the transistor are largely based on the DMILL model (DMILL being the technology used to fabricate the ABCD) for the actual ABCD front-end transistor, but we adjusted the base-emitter resistance to 18 Ω to match the response to the short zapper pulse seen in Figure 4 (left). The large resistor and the Zener diode model the breakdown and recovery

seen in Figure 4 (right). The Zener diode controls the fast recovery to -2 V, and the large resistor models the slower recovery to 0 V. Lowering the base-emitter resistance from that of the original DMILL model is reasonable given that the voltage ranges at the base far exceed those expected for the small signal models. The remaining breakdown current paths in the real ABCD are not well understood, so our model is based on accurately reproducing the available data for these conditions outside the normal operating regime of the IC.

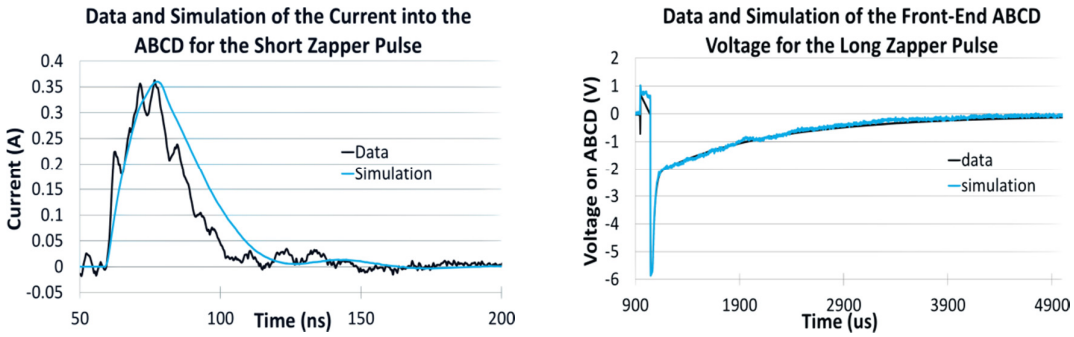

Figure 4: Data and simulation of the ABCD response to voltage signals.

3. Beam loss simulation sequence

3.1 Beam loss in the LHC

Previous beam loss simulations found that in a scenario where 0.1 % of the LHC beam scrapes a TAS collimator, there would be a rather uniform particle flux of up to 5.4 x 10^5 MIPs/strip/bunch crossing across each SCT barrel module. In this study, we assume that this rise in particle flux occurs linearly over various time profiles ranging from 100 ms to 10 ns. We further assume that a beam dump is triggered at the end of this initial rise, but that the beam continues to deviate at the same rate during a 90 μs beam dump sequence.

Since both the percentage of beam that scrapes the collimator and the time over which the beam loss occurs may vary in practice, we define a "rate of beam loss" with units of MIPs/bunch/second to summarize our results. We find that in all cases studied the performance parameters depend on the rate of the beam loss rather than its duration. Thus, our results should be applicable to a wide range of beam loss scenarios.

3.2 Charge collection in the silicon sensors

For a given charge, Q, deposited in silicon sensors, the charge collection time, t_{cc}, scales as $\sqrt[3]{Q}$ [9]. In our silicon sensors, the expected relationship is

$$t_{cc} = 10\ ns * \sqrt[3]{MIPs} \quad (2)$$

where $MIPs$ refers to the total number of minimum ionizing particles that pass through the sensor at a given time, and 10 ns is a typical response time for a single MIP. This means that for rates above 15 MIPs/strip/bunch crossing, the charge collection time surpasses the 25 ns bunch spacing in the LHC, and successive pulses will overlap, causing a continuous current to be deposited in the implant strips.

A simple interpolating algorithm is used to approximate the current values for overlapping pulses. We use a linear function whose slope is determined by the expected particle flux at the time the beam is dumped along with the time scale over which the beam loss occurs. We then move along the time axis in steps of 25 ns. At each step, we use our function to

determine the expected number of MIPs, and convert this to an expected charge (in Coulombs) according to the charge deposition for a given sensor thickness,

$$Q = MIPs * 80 \frac{e^-}{\mu m} * 289.5\ \mu m * 1.6 * 10^{-19} \frac{C}{e^-} \quad (3)$$

We also calculate t_{cc}, as in equation 2, and use both of these to determine the expected current from each bunch crossing. Using a resolution of 1 ns, an array stores all current contributions at a particular time in the simulation. We then fit a line to these time-current data points, and use this function in the current sources that connect the backplane to the implant strips.

4. Results

4.1 The 10 ms beam loss scenario

The beam loss simulation results from different time scales are all qualitatively similar, but differ only in their time scales and the magnitude of currents and voltages. In this section we present the full set of results for the 10 ms beam loss scenario. In section 4.2, we summarize the primary values of interest for all beam loss scenarios considered.

In Figure 5 we see that shortly after the onset of beam loss, the bias voltage of the sensors quickly drops to close to 0. Even at just 50 μs into the 10 ms simulation, the bias voltage is already below its full depletion value (150 V). Since we expect all strips on a given module to collect the same amount of charge, the large current quickly drains the available charge from the bias filter capacitors. Additionally, the current limit on the power supply reduces the rate at which this charge can be replenished, so a rapid drop in bias voltage is observed. Consequently, the charge collected per strip reaches a maximum approximately when the bias voltage drops to its full depletion value. After this time, the decrease in depletion depth dominates over the increase in particle flux, resulting in less charge collected per strip.

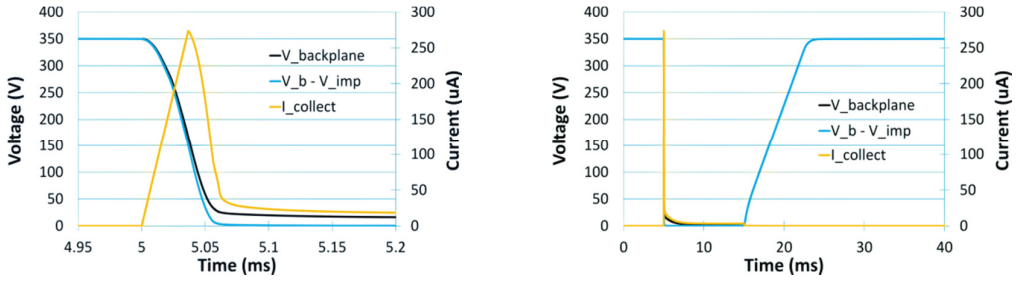

Figure 5: Backplane voltage (dark blue), bias voltage (light blue), and current collected per strip (orange), as functions of time. The left image zooms in on the initial rise in particle flux. The right plot shows the full 10 ms beam loss simulation.

Figure 6 (left) shows that both the coupling capacitor voltage and the current per ABCD channel exhibit behavior similar to the current collected per strip: they reach a maximum approximately when the bias voltage drops to its full depletion value. Beyond this time, they decrease to steady state values until the beam is dumped. In this simulation, the average voltage across the coupling capacitor reaches 25 V, and the maximum ABCD current peaks at 244 μA, equivalent to 6.1 pC in 25 ns. These are both well below the design specifications. Figure 6 (right) shows that the current per ABCD channel is slightly less than the current collected per strip. The excess current escapes to ground through the PTP structure.

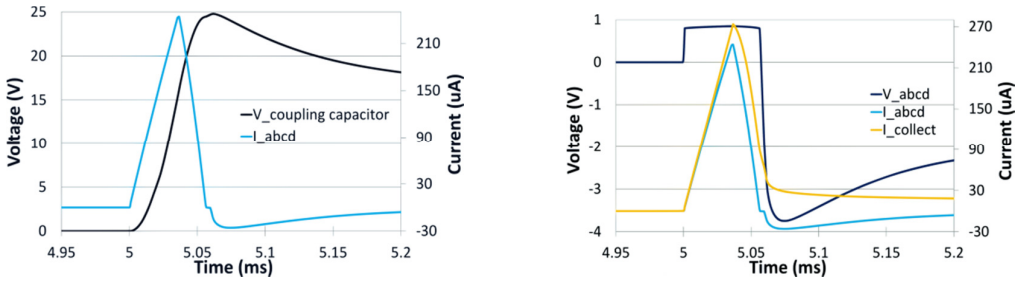

Figure 6: Left: Average voltage across the coupling capacitor (dark blue) and current into the ABCD front end (light blue). **Right:** Voltage at ABCD front end (dark blue), current collected per strip (orange), and current per ABCD channel (light blue).

4.2 Summary of simulations over various time profiles

The two plots in Figure 7 summarize beam loss simulation results in which the particle flux increases from 0 to 5.4 x 10^5 MIPs/strip/bunch over time scales ranging from 100 ms to 10 ns. The particle flux then continues to rise during a 90 μs beam dump. The left hand plot shows the maximum implant voltage on the node furthest from the PTP structure, and the right hand plot shows the peak ABCD current per channel.

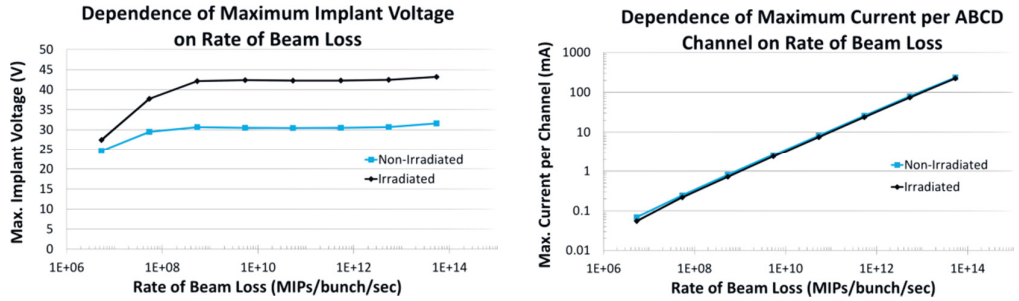

Figure 7: Summary of maximum implant voltage (left) and maximum ABCD current per channel (right) for various time profiles. Non-irradiated sensors are in light blue and irradiated sensors are in dark blue.

In the left side of Figure 7, we see that the maximum implant voltage reaches a plateau for increasing rates of beam loss. This plateau highlights the fact that the module response is strongly influenced by the bias filter characteristics. Since there is initially a finite amount of charge stored in the bias filter, there is a corresponding maximum charge that can be collected by the strips, which limits the voltage across the coupling capacitor. For non-irradiated strips, the voltage plateaus at 30 V and for irradiated strips, the voltage plateaus at 43 V. This difference is relatively small, since higher bias voltage for irradiated sensors corresponds to higher full depletion voltage. Both values are significantly smaller than specification for the entire simulated range of beam loss rate spanning 7 orders of magnitude.

The right plot in Figure 7 shows that the maximum ABCD current per channel rises with increasing rates of beam loss. However, the ABCD specification is only exceeded for beam loss rates in excess of 10^{13} MIPs/bunch/sec. The observed relationship is $I_{max} \propto \sqrt{R}$, where R is the beam loss rate, and I_{max} is the maximum ABCD current per channel. This relationship can be explained as follows: first we observe that R has units of MIPs/bunch/sec. If we convert MIPs to a corresponding charge Q and recall that the bunch spacing is 25 ns, then R has equivalent units of C/s^2, which is a rate of increase in current. Thus, the current collected by the strips at a

given time is given by $I(t) \propto R * t$, where t is the time elapsed from the onset of beam loss. Taking the time integral of this current, we find that the total charge collected by the strips is given by $Q(t) \propto R * t^2$. In Figure 5, the collected charge per strip peaks approximately when the bias voltage drops below the full depletion value. Ignoring contributions from the power supply, the amount of charge that can be collected before this voltage is reached is given by, $Q_{max} = C_{total}(V_{bias,inital} - V_{fd})$, where C_{total} is the total capacitance of the bias filter. This charge is fixed by the operational bias voltage. To finish, we solve for t_{max}, such that $Q(t_{max}) = Q_{max}$. Plugging it into $I(t)$, we find that $I_{max} = I(t_{max}) \propto \sqrt{R}$.

5. Laser pulse studies

Previous studies have used laser pulses to evaluate potential damage to the ATLAS SCT during beam loss scenarios [5,10,11]. In these studies, a laser delivers a high intensity pulse to a small spot affecting a few strips on a sensor. For simplicity, we simulate this scenario by injecting 5.4 x 10^5 MIPs to a single implant node in our SPICE model and compare the results to our realistic beam loss simulations above.

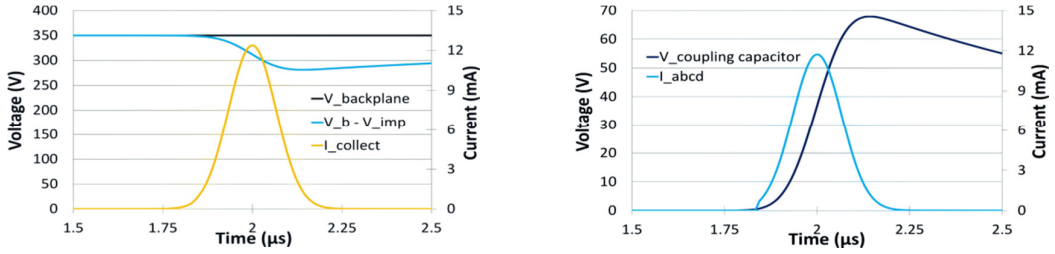

Figure 8: These two plots show the same traces as Figures 5 and 6 from the 10 ms beam loss scenario, but the results here are from laser pulse simulations.

On the left side of Figure 8, we see that in the laser pulse simulation, the backplane voltage (dark blue) is maintained at 350 V. Since only one strip is collecting charge in this case, and the charge is a single, high intensity pulse, rather than a succession of pulses of increasing intensity, the amount of charge drained from the bias filter is many orders of magnitude less than in the beam loss simulations. The result is that the bias voltage drops somewhat due to an increasing voltage on the implant strip, but still remains above its full depletion value. On the right side of Figure 8, we see that the coupling capacitor voltage reaches nearly 70 V, and the ABCD current peaks at 11.7 mA, equivalent to 0.3 nC in 25 ns. The module behavior in this scenario is very different from our beam loss simulations, indicating that the distributed particle flux and high charge injection frequency are important. The laser studies don't have these features. They may address properties of the sensor structures but not the full effect on SCT modules.

6. Conclusion

Our simulations show that during the most likely beam loss scenarios, namely, when the particle flux across an ATLAS SCT barrel module is rather uniform, there exist inherent self-protection features in the barrel module electrical system. These self-protection features are the finite amount of charge stored on the bias filter capacitors and the power supply current limit. Endcap modules have a similar bias filter, so we expect these features to work similarly in that system. Because of these features, the bias filter is unable to maintain a sufficient bias voltage during realistic beam loss scenarios. As a result, the amount of charge collected by the

implant strips is limited due to a reduced depletion depth in the sensors. We find that during these beam loss scenarios, the coupling capacitor voltage never approaches its breakdown specification over the entire range of beam loss rates studies. The current per ABCD channel only reaches its specified limit for beam loss rates in excess of 10^{13} MIPs/bunch/second. In cases where only a fraction of the strips on a given SCT module are subjected to a large particle flux, e.g. when a single strip is zapped by a laser, these self-protection features are not actuated, and the observed behavior of the module is very different. Therefore, these sorts of studies may not address the full complexity of SCT module response during beam loss. However, since small variations in particle flux across the strips in a single SCT module may exist, it would be useful to investigate what effect these variations have on the observed behavior of the modules.

Acknowledgments

Special thanks to J. Kaplon from the CERN microelectronics group and W. Dabrowski from AGH University for helpful consultations, C. Haber from LBL for providing the SCT sensors, and the U. of Sydney group for discussions regarding their simulations.
Work supported by the U.S. Dept. of Energy under grant DE-FG02-13ER41983.

References

[1] ATLAS Collaboration, 2008 JINST 3 S08003.

[2] A. Abdesselam et al., The barrel modules of the ATLAS semiconductor tracker, Nucl. Instrum. Methods A568 642 (2006).

[3] F. Campabadal et al., Design and performance of the ABCD3TA ASIC for readout of silicon strip detectors in the ATLAS semiconductor tracker, Nucl. Instrum. Methods A552 292 (2005).

[4] A. Kuhl et al., ATLAS ABCD hybrid fatal charge dosage test, 2011 JINST 6 C12021.

[5] K. Hara et al., Beam splash effects on ATLAS silicon microstrip detectors evaluated using 1-w Nd : YAG laser, Nucl. Instrum. Methods A541 15 (2005).

[6] N. Patel et al., Charge deposition in the SCT due to beamloss, ATLAS Note ATL-INDET-PUB-2013-002.

[7] LTSpice is a free implementation of SPICE circuit simulator, provided by Linear Technology Corp. As of October 7, 2013, it is available at http://www.linear.com/designtools/software/ .

[8] D. Robinson et al, Silicon microstrip detectors for the ATLAS SCT, Nucl. Instrum. Methods A 485 (2002) 84.

[9] W. Seibt, K.E. Sunstrom, and P.A. Tove, Charge Collection in Silicon Detectors for Strongly Ionizing Particles, Nucl. Instrum. Methods 113 (1973) 317.

[10] H.F.-W. Sadrozinski et al., Punch-through protection of SSDs, Nucl. Instrum. Methods A699 31 (2013).

[11] C. Betancourt, et al., The Punch-Through Effect in Silicon Strip Detectors, IEEE Trans. Nucl. Science, 59 (2012) 671